tained in tables of atom positional parameters, least squares planes, and anisotropic thermal parameters, and solution thermodynamic material contained in figures of observed and calculated dependent variables for the spectrophotometric titration of the bicapped-TRENCAM ligand, observed and calculated chemical shifts for the NMR titration of the bicappedTRENCAM ligand, observed and calculated dependent variables for spectrophotometric titration of the Fe(bicappedTRENCAM) complex, and plot of absorbance vs time for the competition experiment with CDTA and Fe(bicappedTRENCAM) (13 pages); table of observed and calculated structure factors (13 pages). Ordering information is given on any current masthead page.

Spectroscopic Studies of the Electronic Structure of Iron(III) Tris(catecholates)

Timothy B. Karpishin,[†] Matthew S. Gebhard,[§] Edward I. Solomon,*[,§] and Kenneth N. Raymond*[,†]

Contribution from the Department of Chemistry, University of California, Berkeley, California 94720, and Department of Chemistry, Stanford University, Stanford, California 94305. *Received August 31, 1990*

Abstract: Single-crystal polarized absorption and magnetic circular dichroism (MCD) have been employed to elucidate the electronic structure of the iron(III) tris(catecholate) complex $[Fe(cat)_3]^{3-}$ to investigate the bonding in ferric enterobactin and similar catechol siderophores. In addition to $[Fe(cat)_3]^{3-}$, two related complexes, $[Fe(TRENCAM)]^{3-}$, a catecholamide, and $[Fe(eta)_3]^{3-}$, a terephthalamide, have been studied by MCD to provide a perturbation on the electronic structure of $[Fe(cat)_3]^{3-}$ and to also determine differences in bonding between the three complexes. The ligand-to-metal charge-transfer (CT) band characteristic of the catecholate siderophores is found for $[Fe(cat)_3]^{3-}$ to be composed of two overlapping x,y polarized transitions at 18414 and 22018 cm^{-1}. These transitions are ligand π to metal d in nature; assignments of these and four other CT transitions and an experimental energy order for the molecular orbitals of the complexes are made in D_3 symmetry. It is evident from analysis of the spectra that a significant contribution to the Fe–O interaction in these complexes is made by π bonding. An estimate of $10Dq$ as ~ 13000 cm^{-1} is made for the iron(III) tris(catecholates) from the transition energy of the spin forbidden ligand field $(LF)^6A_1 \rightarrow {}^4T_1$ transition observed in the MCD. A value of $10Dq$ is also obtained from the CT transition energies and is determined to be $\sim 63\%$ of the value obtained from the LF transitions. This reduction indicates that the CT excited state is best described as an iron(II) species. Analysis of the CT spectra indicates that the electronic structure of the two complexes $[Fe(cat)_3]^{3-}$ and $[Fe(TRENCAM)]^{3-}$ are similar, whereas $[Fe(eta)_3]^{3-}$ shows a higher degree of σ and π interactions in Fe–O bonding. The contribution of differences in bonding to the known thermodynamic stability constants is discussed.

In response to the challenge posed by iron requirement and unavailability, microorganisms secrete high-affinity iron-binding compounds called siderophores.[1-4] The siderophores are powerful chelating agents which typically use hydroxamate (R–N(O^-)C(O)–R′) or catecholate groups to coordinate the ferric ion octahedrally. The characterization of the physical properties of siderophores and their synthetic analogues are of interest because of their high selectivity for iron(III), and in the case of the tris(catecholates), their remarkable thermodynamic stability ($K_f > 10^{40}$).[5] One striking characteristic of these iron complexes is their intense red color (the original name siderochrome referred to this color), which is attributable to spin-allowed ligand-to-metal charge-transfer (CT) transitions. Although the CT spectra of the siderophores and their analogues have been used extensively as fingerprints to measure stability constants,[5-7] to follow the kinetics of Fe removal from transferrin,[8] and to elucidate protonation behavior,[9] a detailed assignment of the observed transitions has not appeared. The visible spectra of the tris(hydroxamate) (e.g., ferrichrome A) and the tris(catecholate) (e.g., enterobactin) siderophores are generally dominated by one broad intense band at 20000–22000 cm^{-1}.[1,10] The similarity between these visible spectra would indicate common features for the electronic structure of these chromophores. The goal of this study is to elucidate the electronic structure in iron(III) tris(catecholates) and thus determine the contribution of the electronic structure to the high-affinity bonding in the catecholate siderophores.

The iron(III) tris(catecholate) complex, $[Fe(cat)_3]^{3-}$, is a simple model for ferric enterobactin[11,12] (Figure 1) having a similar visible spectrum[13] and also very high thermodynamic stability.[5,14] Although assignment of the CT bands in $[Fe(cat)_3]^{3-}$ has been previously addressed,[13] there has been only one thorough study of the electronic structure of the complex.[15] The authors of the

[†] University of California, Berkeley.
[§] Stanford University.

(1) Matzanke, B. F.; Müller-Matzanke, G.; Raymond, K. N. In *Iron Carriers and Iron Proteins*; Loehr, T. M., Ed.; Physical Bioinorganic Series; VCH Publishers: New York, 1989; pp 1-121.
(2) Raymond, K. N.; Carrano, C. J. *Acc. Chem. Res.* **1979**, *12*, 183.
(3) Raymond, K. N.; Müller, G.; Matzanke, B. F. *Top. Curr. Chem.* **1984**, *123*, 49.
(4) Neilands, J. B. *Ann. Rev. Biochem.* **1981**, *50*, 715.
(5) Avdeef, A.; Sofen, S. R.; Bregante, T. L.; Raymond, K. N. *J. Am. Chem. Soc.* **1978**, *100*, 5362.
(6) Harris, W. R.; Carrano, C. J.; Cooper, S. R.; Sofen, S. R.; Avdeef, A. E.; McArdle, J. V.; Raymond, K. N. *J. Am. Chem. Soc.* **1979**, *101*, 6097.
(7) Garrett, T. M.; Miller, P. W.; Raymond, K. N. *Inorg. Chem.* **1989**, *28*, 128.
(8) Kretchmar, S. A.; Raymond, K. N. *J. Am. Chem. Soc.* **1986**, *108*, 6212.
(9) Cass, M. E.; Garrett, T. M.; Raymond, K. N. *J. Am. Chem. Soc.* **1989**, *111*, 1677.
(10) Raymond, K. N.; Abu-Dari, K.; Sofen, S. R. In *Stereochemistry of Optically Active Transition Metal Compounds*; Douglas, B. E., Saito, Y., Eds.; ACS Symposium Series No. 119; American Chemical Society: Washington, DC, 1980; pp 133-167.
(11) Anderson, B. F.; Buckingham, D. A.; Robertson, G. B.; Webb, J.; Murray, K. S.; Clark, P. E. *Nature* **1976**, *262*, 722.
(12) Raymond, K. N.; Isied, S. S.; Brown, L. D.; Fronczek, F. R.; Nibert, J. H. *J. Am. Chem. Soc.* **1976**, *98*, 1767.
(13) Salama, S.; Stong, J. D.; Neilands, J. B.; Spiro, T. G. *Biochemistry* **1978**, *17*, 3781.
(14) Loomis, L. D.; Raymond, K. N. *Inorg. Chem.*, in press.
(15) Gordon, D. J.; Fenske, R. F. *Inorg. Chem.* **1982**, *21*, 2916.

0002-7863/91/1513-2977$02.50/0

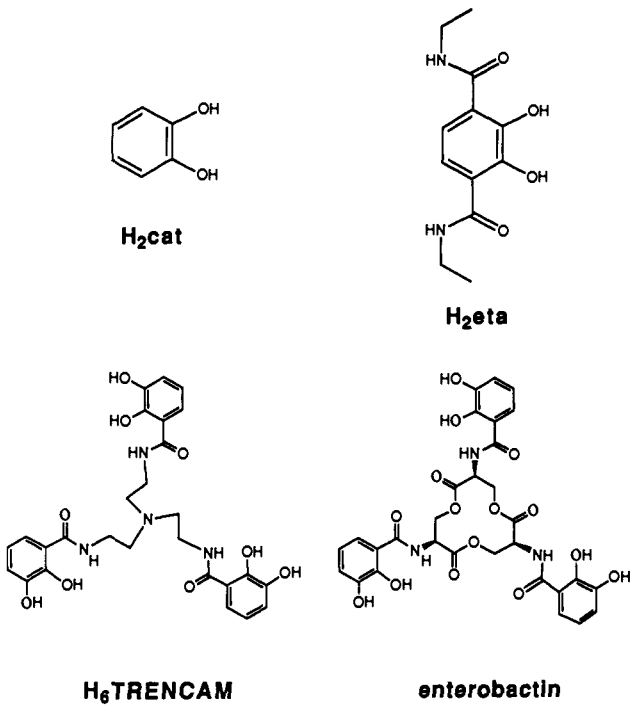

Figure 1. Ligands used in this study: catechol, H_2cat; 2,3-dihydroxyethylterephthalamide, H_2eta; $H_6TRENCAM$. Also shown is the siderophore enterobactin.

latter study concluded from Fenske–Hall molecular orbital calculations that $[Fe(cat)_3]^{3-}$ has an $S = 1/2$ ground state although EPR,[5] variable temperature magnetic susceptibility,[11] and Mössbauer[16] data indicate that the complex is high spin ($S = 5/2$).

In the present study, low-temperature single-crystal-polarized absorption and magnetic circular dichroism (MCD), combined with vector-coupling selection rules, have been employed to assign definitively the excited-state electronic structure and experimentally determine the energy levels of the molecular orbitals in the $[Fe(cat)_3]^{3-}$ complex. A recent study has used the same protocol to elucidate the electronic structure of an oxidized rubredoxin model complex $[Fe(SR)_4]^-$ (R = 2,3,5,6-$(Me)_4C_6H$).[17] The crystal structure of $K_3[Fe(cat)_3]\cdot 1.5H_2O$ has been previously determined[12] and shows that the coordination sphere of the $[Fe(cat)_3]^{3-}$ anion is distorted from octahedral. Although 3-fold symmetry is not crystallographically imposed on the complex in the solid state, it has, in effect, D_3 symmetry. For a high-spin d^5 complex with D_3 symmetry, the ground state is $^6A_1$, and ligand-to-metal CT transitions can give rise to either of the excited states ^6E or $^6A_2$ (a $^6A_1 \rightarrow {}^6A_1$ transition is forbidden). A molecular orbital calculation (MNDO) on the catechol dianion shows the two HOMOs to be of π symmetry;[18] it is thus expected a priori that the CT bands are resultant from ligand π-to-metal d transitions. None of the $^6A_1 \rightarrow {}^4\Gamma$ spin-forbidden ligand field transitions have ever been observed in the tris(catecholates) since they are weak and are obscured by the intense CT transitions.

The two related complexes $[Fe(TRENCAM)]^{3-}$ and $[Fe(eta)_3]^{3-}$ (Figure 1) have also been investigated by MCD spectroscopy to provide a perturbation (by increasing amide substitution) on the electronic structure of the $[Fe(cat)_3]^{3-}$ complex. The TRENCAM complex was chosen as it is a synthetic analogue of enterobactin.[19] Also, the 2,3-dihydroxyterephthalamides have recently been shown to be the strongest bidentate ligands for Fe^{III} at physiological pH.[7] It was thus hoped that in addition to providing a perturbation on the electronic structure of catechol, the series of complexes could be investigated with the ultimate goal of defining the differences in the electronic structure of the complexes and relating these to variations in bonding.

Experimental Section

Preparation of Compounds. Unless otherwise noted, all chemical starting materials were obtained commercially and used without further purification. All solvents were reagent grade and all preparations of complexes were performed under an inert atmosphere. The ligands H_2eta,[7] $H_6TRENCAM\cdot HBr$[19] and the complex $K_3[Ga(cat)_3]\cdot 1.5H_2O$[20] were prepared according to the published procedures. Elemental analyses were performed by the Microanalytical Laboratory, College of Chemistry, University of California, Berkeley. Analyses that were within 0.4% of the calculated values were considered acceptable. Each of the metal complexes prepared are stable to air in the solid state.

$K_3[Fe(cat)_3]\cdot 1.5H_2O$. The following procedure is a modified version of the published preparation.[12] A solution of $FeCl_3\cdot 6H_2O$ (5.00 g, 18.5 mmol) in 50 mL of H_2O was brought to pH 7 with 4 M NH_4OH, resulting in the precipitation of hydrous ferric oxide. The gelatinous precipitate was washed with H_2O and suspended in 150 mL of H_2O, to which was added catechol (6.32 g, 57.4 mmol, sublimed prior to use). An aqueous KOH solution (115 mmol) was added, and the mixture darkened to a deep red. The reaction was stirred at room temperature for 3 h, the volume was reduced to 50 mL, and EtOH was added to precipitate the product (8.7 g, 95%). Anal. ($K_3FeC_{18}H_{12}O_6\cdot 1.5H_2O$) C, H, Fe.

$K_3[Fe(eta)_3]$. To 0.200 g of H_2eta (0.793 mmol) dissolved in MeOH was added hydrous ferric oxide (0.264 mmol) as a MeOH suspension, and then 8.0 mL of 0.10 M KOH solution. The deep red solution was stirred at room temperature for 30 min and then filtered. Removal of the solvent gave 0.23 g of a deep red microcrystalline solid (93%). Anal. ($K_3FeC_{36}H_{42}O_{12}N_6$) C, H, N.

$(Et_3NH)_3[Fe(TRENCAM)]$. To 0.125 g of $H_6TRENCAM\cdot HBr$ (0.20 mmol) dissolved in MeOH was added 0.070 g of $Fe(acac)_3$ (0.20 mmol) and 0.15 mL of Et_3N (1.1 mmol). The solution was stirred at room temperature for 20 min, the volume was reduced, and Et_2O was added to precipitate the product as a black-red solid (0.15 g, 83%). Anal. ($FeC_{45}H_{72}N_7O_9$) C, H, N.

Single-Crystal-Polarized Absorption Spectra. Polarized absorption spectra were measured on a McPherson RS-10 double beam spectrophotometer described previously[21] but with upgraded electronics. A pair of Glan-Taylor polarizers matched from 200 nm to 2.5 μm were used in the sample and reference beams. A grating blazed at 7500 Å and an extended S-20 photomultiplier tube were used in the energy region from 4000 to 8000 Å. The light source was a tungsten–halogen lamp. A Janis Super-Vari Temp dewar was used for the liquid He temperature absorption experiments.

Single crystals of $K_3[Ga(cat)_3]\cdot 1.5H_2O$ doped with 0.5% of $K_3[Fe(cat)_3]\cdot 1.5H_2O$ were used for the polarized spectra since dilute concentrations of the iron complex are required to record absorption spectra in the visible region. Crystals were grown from 1 M KOH by vapor diffusion of EtOH over a period of several weeks under anaerobic conditions. The crystal structures of the Fe and Ga complexes have been determined previously[12,20] and both crystallize in the monoclinic space group $C2/c$ with unit cell volumes of 4025 and 4050 Å^3, respectively. Isomorphous substitution of the iron complex into the gallium lattice was evident by the even coloring of the crystals. Pale red needles of typical dimensions 1.5 × 2.0 × 6.0 mm were indexed by using an X-ray precession camera. Well formed needles have the (010), (110), (0$\bar{1}$0), ($\bar{1}$10), (1$\bar{1}$0), and ($\bar{1}\bar{1}$0) faces developed, and the needle axis corresponds to the c-axis of the unit cell. Four of each of the Δ and Λ optical isomers (defined for $M(bidentate)_3$ complexes) crystallize in the unit cell with the eight metal atoms occupying general positions. Polarization of the light beam with the E-vector perpendicular and parallel to the c-axis of a crystal gives the x,y and z molecular polarized spectra respectively, since the 3-fold axes of the molecules (defined as the vector between the center of the top trigonal face of oxygen atoms and the center of the bottom trigonal face) lie only 3.2° off of the c-axis in the Ga structure (3.7° in the Fe structure).

Polarized data were recorded on both the (110) and (010) faces of the crystal with light parallel and perpendicular to the c-axis. The (110) face was mounted flush against a quartz window, secured with an optically transparent resin (Crystalbond), and masked off with black electrical tape. The crystal was polished to the desired thickness (~100 μm) by using 9-μm lapping film and a homemade polishing apparatus. The (010)

(16) Hider, R. C.; Mohd-Nor, A. R.; Silver, J.; Morrison, I. E. G.; Rees, L. V. C. *J. Chem. Soc., Dalton Trans.* **1981**, 609.
(17) Gebhard, M. S.; Deaton, J. C.; Koch, S. A.; Millar, M.; Solomon, E. I. *J. Am. Chem. Soc.* **1990**, *112*, 2217.
(18) Garrett, T. M. Ph.D. Thesis, University of California, Berkeley, 1988.
(19) Rodgers, S. J.; Lee, C.-W.; Ng, C. Y.; Raymond, K. N. *Inorg. Chem.* **1987**, *26*, 1622.
(20) Borgias, B. A.; Barclay, S. J.; Raymond, K. N. *J. Coord. Chem.* **1986**, *15*, 109.
(21) Wilson, R. B.; Solomon, E. I. *Inorg. Chem.* **1978**, *17*, 1729.

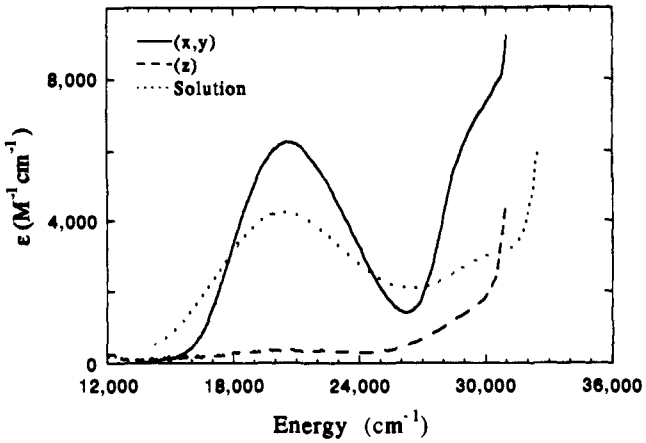

Figure 2. Single-crystal-polarized absorption spectra (110 face) of $K_3[Ga(Fe)(cat)_3]\cdot 1.5H_2O$ ([Fe] = 0.5%) at room temperature (z and solution) and 6 K (x,y).

face is a minor crystal face, and it was therefore necessary to increase the surface area of the face by first polishing down one side of the crystal with the (010) face down and then turning it over and polishing down the opposite face. The axis orientation of the crystals in the sample holder was checked with a polarizing microscope, as the crystals show marked dichroism. When polarized light is propagated with the E-vector perpendicular to the crystal c-axis, the crystal is deep red, whereas it is colorless when the E-vector is polarized parallel to the c-axis.

Magnetic Circular Dichroism Spectra. MCD spectra were recorded on a JASCO J-500C CD spectropolarimeter configured with focussing optics and an Oxford SM4 superconducting magnet capable of producing fields up to 6.0 T at temperatures of 4 K.[22]

Since the space group of the $[M(cat)_3]^{3-}$ complexes is monoclinic (i.e., biaxial), single-crystal MCD spectra could not be recorded.[23] For the three complexes, samples in 1:1 H_2O/saturated aqueous LiCl solution were prepared as these solutions give high quality optical glasses at liquid He temperatures. Solution concentrations were ~0.1 mM to record the charge-transfer spectra and ~30 mM to measure the spin-forbidden d–d bands in the near IR region. Degassed solutions were injected between two quartz discs spaced by a 3-mm rubber spacer and frozen in liquid N_2 before placing them in the sample compartment at 4 K. Depolarization of the beam by the glasses was monitored by the effect each sample had on the CD spectrum of a nickel (+)-tartrate solution placed before and after the sample. Samples which decreased the CD signal by less than 10% were considered suitable. Low-temperature MCD spectra of the $K_3[Fe(cat)_3]\cdot 1.5H_2O$ complex as a mineral oil mull were also taken which were found to be identical with the low-temperature solution (glass) spectra of the complex. This verifies that no structural changes occur in the complex upon dissolving in aqueous LiCl solution.

Results

(I) Single-Crystal-Polarized Absorption of $[Fe(cat)_3]^{3-}$. Single-crystal-polarized spectra of the (110) face of $K_3[Fe(cat)_3]\cdot 1.5H_2O$ doped into $K_3[Ga(cat)_3]\cdot 1.5H_2O$ are shown in Figure 2. The rotationally averaged solution spectrum has two characteristic ligand-to-metal CT bands, one centered at 20 500 cm^{-1} and a shoulder at 30 000 cm^{-1} (absorption at higher energy is due to a ligand centered $\pi \rightarrow \pi^*$ transition). From Figure 2 the lower energy band shows complete x,y polarization, whereas the higher energy shoulder shows both x,y and z polarization.

To determine if the spectra of the complex are best interpreted in terms of D_3 symmetry, polarized data were also recorded on the (010) face. If the x and y molecular axes are equivalent (i.e., the complex is D_3), the (110) and (010) spectra should be identical. The (110) and (010) spectra for the $[Fe(cat)_3]^{3-}$ complex (not shown) were found to be essentially the same, and thus all analyses can be made in D_3 symmetry.

Single-crystal-polarized data were not obtained for either $[Fe(eta)_3]^{3-}$ or $[Fe(TRENCAM)]^{3-}$ due to the inability to grow crystals of sufficient size.

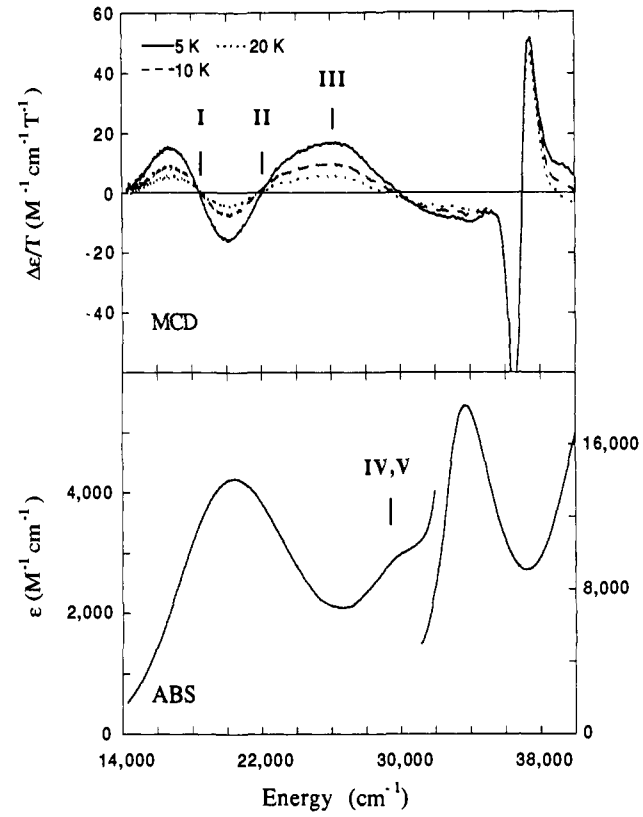

Figure 3. MCD (top) and absorption (bottom) spectra of $[Fe(cat)_3]^{3-}$.

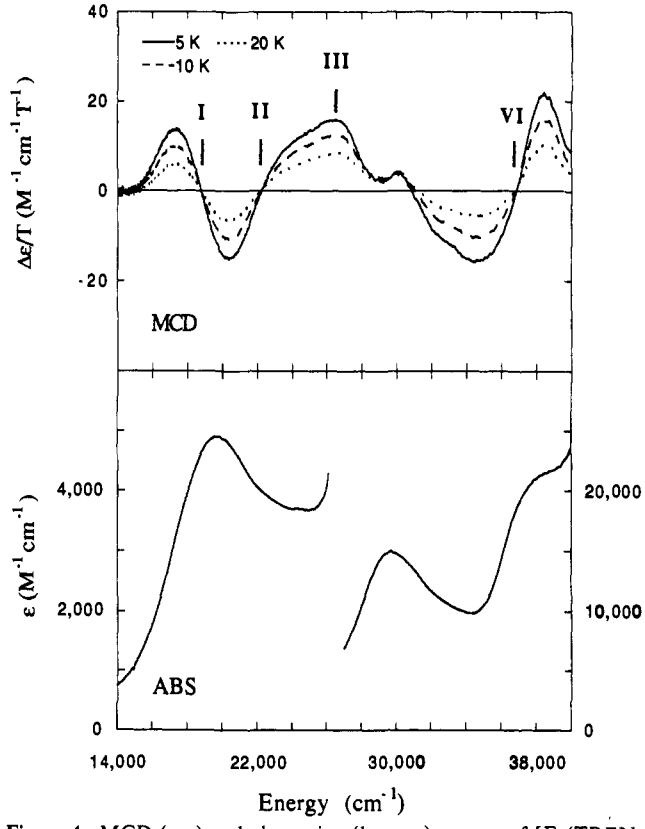

Figure 4. MCD (top) and absorption (bottom) spectra of $[Fe(TRENCAM)]^{3-}$.

(II) Magnetic Circular Dichroism. (a) Charge-Transfer Transitions. Solution MCD spectra of the three complexes were recorded as frozen aqueous glasses at 5–20 K. The MCD spectra of the complexes presented with their solution UV–vis spectra are shown in Figures 3–5. Since the ground state of Fe^{3+} is a degenerate $^6A_1$, features associated with this center should exhibit

(22) Allendorf, M. D.; Spira, D. J.; Solomon, E. I. *Proc. Natl. Acad. Sci. U.S.A.* **1985**, *82*, 3063.

(23) Piepho, S. B.; Schatz, P. N. *Group Theory in Spectroscopy*; Wiley-Interscience: New York, 1983.

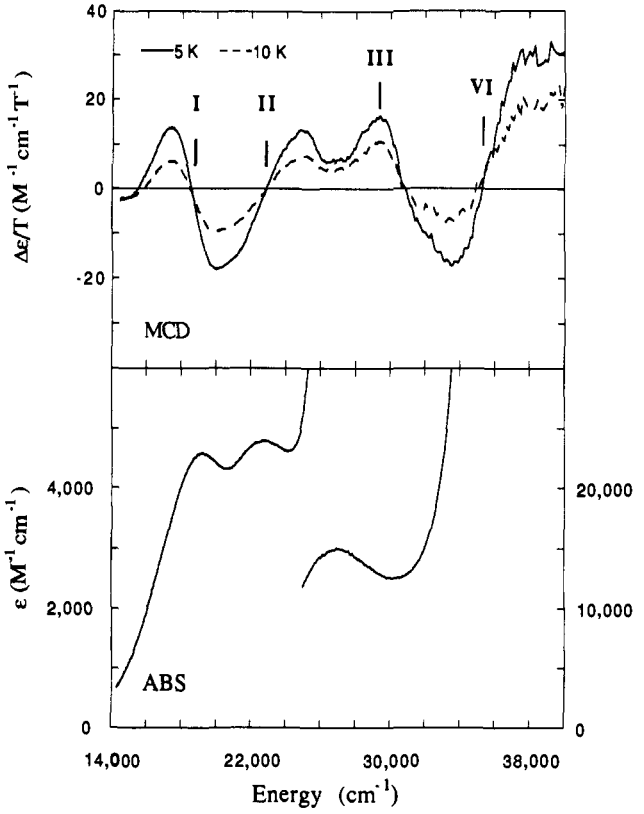

Figure 5. MCD (top) and absorption (bottom) spectra of $[Fe(eta)_3]^{3-}$.

increasing MCD intensity with decreasing temperature (i.e., C-term behavior[24]). For each of the complexes, the higher energy bands (with $\epsilon > 10\,000$ M^{-1} cm^{-1}) in the absorption spectra are ligand-centered transitions ($\pi \rightarrow \pi^*$) and have no temperature-dependent MCD features associated with them, whereas the bands with $\epsilon \approx 4000$ M^{-1} cm^{-1} are the ligand-to-metal CT transitions which have corresponding temperature-dependent MCD features. For the $[Fe(cat)_3]^{3-}$ complex (Figure 3), it was at first surprising that a negative MCD band seems to correspond to the peak at 20 500 cm^{-1} in the absorption spectrum. It was expected (see Analysis section) that since this band is completely x,y polarized (Figure 2) and is thus a CT transition to a ^6E excited state, that the corresponding MCD feature should be a pseudo A term (which is composed of two overlapping temperature-dependent C terms of opposite sign[23]) with its crossover point at 20 500 cm^{-1}. This apparent inconsistency was resolved by correlation with the spectra of the $[Fe(eta)_3]^{3-}$ complex. The absorption spectrum of $[Fe(eta)_3]^{3-}$ shows two ligand-to-metal CT transitions at ~21 000 cm^{-1} separated by 4000 cm^{-1} (Figure 5), and it can be seen that these two bands correspond to two pseudo A terms in the MCD: I is a negative pseudo A and II is a positive pseudo A term. The transitions I and II in $[Fe(cat)_3]^{3-}$ are therefore close enough in energy that the negative components of the two pseudo A terms overlap and appear to be one negative MCD feature. These two transitions also overlap to result in one band at 20 500 cm^{-1} in the absorption spectrum of the $[Fe(cat)_3]^{3-}$ complex (Figure 3). The spectra of $[Fe(TRENCAM)]^{3-}$ (Figure 4) are similar to the $[Fe(cat)_3]^{3-}$ complex where I and II overlap in both the MCD and absorption spectra.

In $[Fe(cat)_3]^{3-}$ and $[Fe(TRENCAM)]^{3-}$, there is an additional positive MCD C term (band III) at ~26 000 cm^{-1} which is a shoulder on the pseudo A term II. This band is shifted to 29 300 cm^{-1} and better resolved in $[Fe(eta)_3]^{3-}$. There is no band in the absorption spectra of each of the complexes which corresponds to band III seen in the MCD spectra. In the MCD spectrum of the $[Fe(TRENCAM)]^{3-}$ complex there is a small peak at 30 000 cm^{-1} which is temperature independent and must therefore be a ligand-centered transition.

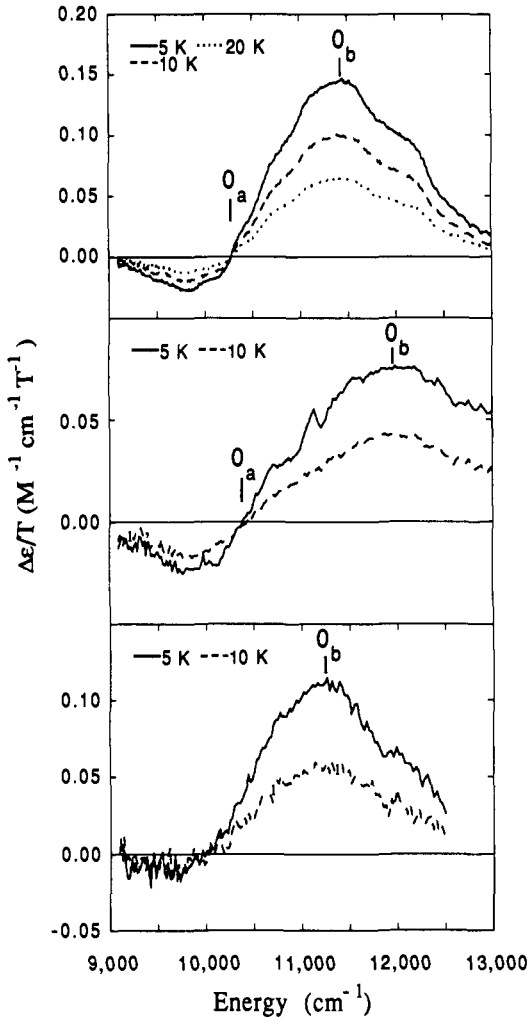

Figure 6. MCD spectra of the ligand field transitions of $[Fe(cat)_3]^{3-}$ (top), $[Fe(TRENCAM)]^{3-}$ (center), and $[Fe(eta)_3]^{3-}$ (bottom).

We attribute two bands (IV and V) to the shoulder seen in the absorption spectrum of $[Fe(cat)_3]^{3-}$ (Figure 3) since it is both x,y and z polarized and must then correspond to two different excited states (see Analysis section). Bands IV and V are not observed in the absorption spectra of either of the other two complexes as the bands are obscured by the lower energy $\pi \rightarrow \pi^*$ transitions. Bands IV and V are also not observed in the MCD spectra of any of the three complexes.

At still higher energy, it is possible with low-temperature MCD to probe ligand-to-metal CT transitions that are completely obscured by very intense ligand-centered transitions in the absorption spectra. In the complexes $[Fe(eta)_3]^{3-}$ and $[Fe(TRENCAM)]^{3-}$ a positive pseudo A term (band VI) is seen at 35 280 and 36 900 cm^{-1}, respectively. In $[Fe(cat)_3]^{3-}$ we see an A term at 37 500 cm^{-1} which is temperature independent and must therefore be a ligand-centered transition. There does appear however to be a positive temperature-dependent pseudo A term under this ligand transition centered at ~37 000 cm^{-1} which corresponds to band VI in the other two complexes.

(b) Ligand Field Transitions. The spin forbidden d–d bands are not observed in the absorption spectra of any of the tris(catecholates) as they are weak and obscured by the highly intense CT transitions. In the low-temperature MCD spectra however, ligand field (LF) transitions, although quite weak, can be seen by using very concentrated samples. MCD spectra were recorded for each of the complexes as frozen aqueous glasses at 5–20 K and at concentrations of ~30 mM; these are shown in Figure 6. Two transitions are assigned for these LF bands in the three complexes (see Analysis section); a positive pseudo A term (0_a)

(24) Stephens, P. J. *Adv. Chem. Phys.* **1976**, *35*, 197.

Table I. Spectral Data (in cm^{-1}) and Assignments

band	assignment	$[Fe(cat)_3]^{3-}$	$[Fe(TRENCAM)]^{3-}$	$[Fe(eta)_3]^{3-}$
		LF Transitions		
0_a	$^6A_1 \rightarrow {}^4E$	10300	10400	
0_b	$^6A_1 \rightarrow {}^4A_2$	11400	12000	11200
		LMCT Transitions		
I	$a_2 \rightarrow e^a$	18414	18783	18587
II	$e_{\pi 1} \rightarrow e^a$	22018	22278	22883
III	$a_2 \rightarrow e^b$	25761	25976	29326
IV, V	$e_{\pi 1} \rightarrow e^b$	30300		
VI	$a_1 \rightarrow e^a$	~37000	36900	35280

and a positive C term (0_b) at higher energy. In both $[Fe(cat)_3]^{3-}$ and $[Fe(TRENCAM)]^{3-}$, band 0_a is centered at ~10400 cm^{-1}; however, the data for $[Fe(eta)_3]^{3-}$ are too noisy in this region to determine the location of this band. Band 0_b shifts somewhat for each of the complexes, occurring at 12000 cm^{-1} for $[Fe(TRENCAM)]^{3-}$.

Each of the MCD spectra were modelled with a Gaussian fitting program[17] to determine accurately the transition energies; the spectral data are summarized in Table I.

Analysis

It is evident from the highly polarized nature of the charge-transfer transitions (bands I and II) in the $[Fe(cat)_3]^{3-}$ single-crystal spectra (Figure 2) that the effective site symmetry is less than octahedral for this complex. Although the actual site symmetry is C_1, the polarized absorption data on the (010) and (110) faces indicate that the effective site symmetry is D_3, and the analysis of the polarized absorption and MCD spectra is carried out in the D_3 point group. While there are no polarized absorption data on the other two complexes, they are treated as having D_3 site symmetry based on strong spectral similarities to $[Fe(cat)_3]^{3-}$.

Figure 7 gives the molecular orbital diagram for iron(III) tris(catecholates) showing the Fe 3d orbitals and the two highest sets of catecholate valence orbitals (π_1 and π_2). The observed charge-transfer spectra (Figures 3–5) are expected to arise from transitions between these cat_π and the Fe 3d orbitals, with the lowest energy charge-transfer transitions coming from the π_1 set. Both of these ligand valence sets involve the out-of-plane π orbitals of the catecholate and are mostly π bonding with respect to the Fe 3d orbitals. The cat σ bonding valence orbitals are at deeper energy and thus are not included in Figure 7, as they do not contribute to the observed charge-transfer spectra (Figures 3–5).

(I) Selection Rules. (a) Charge-Transfer Transitions. In D_3 symmetry the Fe 3d orbitals transform as an a_1 and two e sets (e^a and e^b). The π_1 and π_2 ligand valence orbitals will be comprised of symmetry-adapted linear combinations which transform as a_2, $e_{\pi 1}$ and a_1, $e_{\pi 2}$, respectively (Figure 7). There are 12 possible one-electron transitions ($a_1 \rightarrow a_1$, $a_1 \rightarrow e^{a,b}$, $a_2 \rightarrow a_1$, $a_2 \rightarrow e^{a,b}$, $e_{\pi 1,\pi 2} \rightarrow a_1$, $e_{\pi 1,\pi 2} \rightarrow e^{a,b}$); only the $a_1 \rightarrow e^{a,b}$, $a_2 \rightarrow a_1$, $a_2 \rightarrow e^{a,b}$, $e_{\pi 1,\pi 2} \rightarrow a_1$, and $e_{\pi 1,\pi 2} \rightarrow e^{a,b}$ transitions are electric dipole allowed. The $a_1 \rightarrow e^{a,b}$, $a_2 \rightarrow e^{a,b}$, and $e_{\pi 1,\pi 2} \rightarrow e^{a,b}$ transitions give rise to x,y polarized ^6E excited states, while the $a_2 \rightarrow a_1$, and $e_{\pi 1,\pi 2} \rightarrow e^{a,b}$ transitions give rise to z polarized $^6A_2$ excited states. An e $\rightarrow$ e transition gives rise to a $^6A_1$, $^6A_2$, and a ^6E state. In principle these states can occur at different energies due to differences in electron repulsion for each multielectron state; however, this involves repulsion terms between a hole localized on the metal and a hole localized on the ligand, and these splittings will tend to be small.

On the basis of the polarized absorption spectrum on $[Fe(cat)_3]^{3-}$ (Figure 2) the x,y polarized transitions labeled I and II must come from either the $a_1 \rightarrow e^{a,b}$, $a_2 \rightarrow e^{a,b}$ or $e_{\pi 1,\pi 2} \rightarrow e^{a,b}$ transitions. It is not possible based on the polarized absorption alone to assign the multielectron state to a specific one-electron transition; however, the MCD spectra of these complexes allow a definitive spectral assignment.

In the absence of spin-orbit coupling only the x,y polarized $^6A_1 \rightarrow {}^6E$ transitions will exhibit MCD features. This is because a transition must be polarized in two perpendicular directions in order to give rise to an MCD feature.[24] While the lack of orbital degeneracy of the ground state precludes the presence of temperature-dependent C terms, as can be seen in Figures 3–5, the low-temperature MCD spectra of these complexes are in fact dominated by temperature-dependent C and pseudo A terms. This temperature-dependent behavior of the MCD features derives from spin-orbit coupling[17] which provides a mechanism for the $^6A_1 \rightarrow {}^6E$ transitions to give rise to pseudo A terms, comprised of two oppositely signed C terms. This also causes the $^6A_1 \rightarrow {}^6A_1$ and $^6A_1 \rightarrow {}^6A_2$ transitions to gain x,y polarized intensity through spin-orbit coupling to the ^6E states allowing them to also gain C term activity.

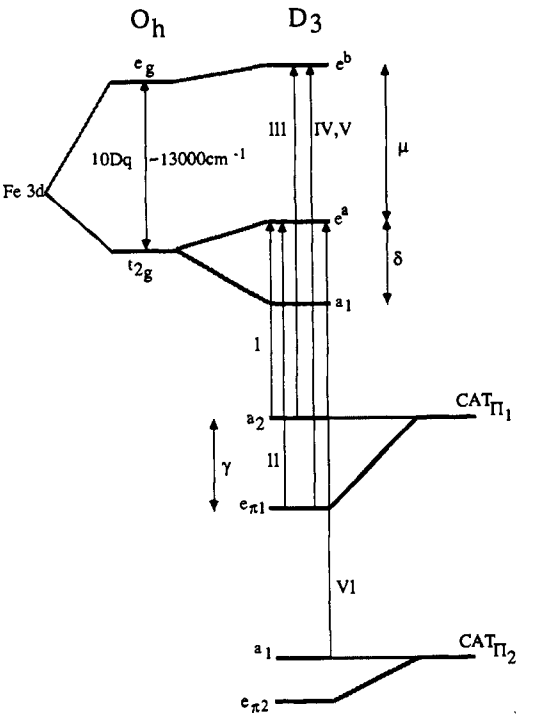

Figure 7. One-electron molecular orbital energy level diagram for iron(III) tris(catecholates). The observed charge-transfer transitions are indicated by arrows and labeled with appropriate Roman numerals.

The ^6E states will exhibit an in-state spin-orbit splitting of the 12-fold degenerate ^6E into six equally spaced doubly degenerate states (3E′ and 3E″ in the D_3 double group). The energy spacing between the doublets is $(1/5)\lambda$, where λ is the multielectron spin-orbit coupling constant. The in-state spin-orbit splitting of a ^6E with a positive λ is presented in Figure 8 along with the wave functions in the uncoupled and coupled representations. The ^6E states must involve an e molecular orbital as either a donor or acceptor in the transition. The magnitude of λ will depend[17] on the specific e molecular orbital (e^a, e^b, $e_{\pi 1}$, or $e_{\pi 2}$) involved in the transition, while the sign of λ depends on the symmetry of the other orbital involved in the transition. For the $a_1 \rightarrow$ e and e $\rightarrow$ e transitions the sign of λ is negative, and for the $a_1 \rightarrow$ e transition the sign of λ is positive. The magnitude of λ is given by eq 1.

$$|\lambda| = \sqrt{\frac{21}{5}}(\langle e||H_{so}||e\rangle) = (\overline{\zeta_{Fe^{3+}}}) \qquad (1)$$

The reduced matrix element is the in-state spin-orbit coupling present in the doubly degenerate one-electron orbital $|e\rangle$ which is either the donor or acceptor in the transition. $\overline{\zeta_{Fe^{3+}}}$ is the effective one-electron spin-orbit coupling constant. If the wave functions, $|e\rangle$, contain pure Fe^{3+} 3d orbitals, then $\overline{\zeta_{Fe^{3+}}} = 430$ cm^{-1}.

The wave functions, $|e\rangle$, in the above matrix element are in fact multicenter functions, with both metal and ligand SALC contributions. Since spin-orbit coupling is a localized one-center operator, contributions which occur between different centers can be neglected. In addition, the oxygen contribution to spin-orbit coupling will be small. Therefore, only the metal character present

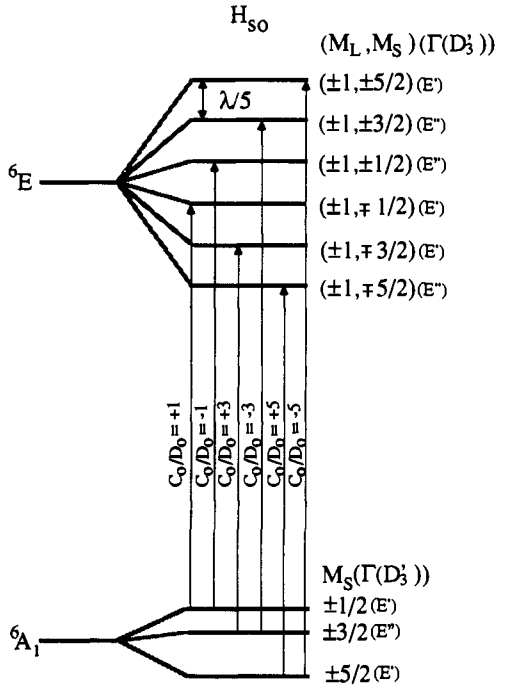

Figure 8. ^6E excited-state in-state spin-orbit splitting along with the wave functions and theoretical C_0/D_0 ratios for the transitions from the zero field split (ZFS) ground-state levels to the spin-orbit components of the ^6E. The ZFS of the ground state is not drawn to scale.

in $|e\rangle$ should contribute significantly to the magnitude of λ. There are two Fe 3d orbitals sets which transform as e, but only the e^a orbital in Figure 7 has in-state orbital angular momentum as it is derived from the octahedral t_{2g} set, thus only the e^a orbital will have a significant spin-orbit coupling parameter. Therefore the observation of a significant spin-orbit splitting indicates that the e^a set must be involved in the transition.

For a paramagnetic molecule at low temperature the MCD signal is described[24] by eq 2. γ depends on constants such as the

$$\left(\frac{\Delta A}{E}\right) = \frac{\gamma C_0 \mu_B B f(E)}{kT} \tag{2}$$

dielectric constant and refractive index, μ_B is the Bohr magneton, B is the external magnetic field, $f(E)$ is an energy-dependent band-shape function, and C_0 is given by eq 3. α, α', λ, and λ'

$$C_0 = -\frac{1}{|A|}\sum_{\substack{\alpha\lambda \\ \alpha'\lambda'}} \langle A\alpha'|(L_z + 2S_z)|A\alpha\rangle [\langle A\alpha|\mathbf{m}_{-1}|J\lambda\rangle \langle A\alpha'|\mathbf{m}_{-1}|J\lambda'\rangle^* - \langle A\alpha|\mathbf{m}_{+1}|J\lambda\rangle \langle A\alpha'|\mathbf{m}_{+1}|J\lambda'\rangle^*] \tag{3}$$

are components of the irreducible representations A (ground state) and J (excited state), $|A|$ is the total degeneracy of the ground state ($|A| = 6$), and $\langle A\alpha|m \pm 1|J\lambda\rangle$ is the dipole matrix element for absorption of right (+) or left (−) circularly polarized light. The MCD selection rules given in Figure 8 for a transition from a spin component of the ground state to a spin-orbit component of the ^6E excited state were derived by using the D_3 double group vector coupling tables and the formalism of Piepho and Schatz.[23] If the spin-orbit components could be resolved, the MCD signal would appear as two sets of three C terms with the following relative magnitudes, 5:3:1:−1:−3:−5. The sign of the highest energy C term depends on the sign of the spin-orbit coupling constant, λ. When the band width is much larger than the spin-orbit splitting, as is the case for this complex, the MCD signal will appear as a derivative-shaped temperature-dependent pseudo A term. When the spin-orbit splitting is small then the spin-orbit components of the ^6E excited state will cancel each other and no pseudo A term will be observed. Thus the magnitude of the MCD is directly related to the magnitude of the in-state spin-orbit splitting, and the observation of a pseudo A term indicates the transition involves the e^a orbital. On the basis of these selection rules a positive λ gives a negative pseudo A term, whereas a negative λ will lead to a positive pseudo A term. The MCD pseudo A term selection rules for the symmetries of the three possible one-electron transitions leading to ^6E states are given in Table II.

Table II. MCD Pseudo A Term Selection Rules

one-electron transition	sign of pseudo A term
$e \rightarrow e$	+
$a_1 \rightarrow e$ or $e \rightarrow a_1$	+
$a_2 \rightarrow e$	−

(b) Ligand Field Transitions. To first order the spin-forbidden ligand field $^6A_1 \rightarrow {}^4\Gamma$ transitions will not be observed in the spectra of these complexes. These transitions will gain intensity through spin-orbit coupling of $^4T_1$ excited-state character into the $^6A_1$ ground state and spin-orbit coupling of $^6T_1$ charge-transfer character into the $^4\Gamma$ excited state. This mechanism also causes these transitions to gain MCD C term activity. This mechanism[17] is described by eq 4. H_{so} is the spin-orbit operator, M_q is the

$$\langle {}^6A_1 M_s|M_q|{}^4\Gamma h M'_s\rangle = \frac{\langle {}^6A_1 M_s|H_{so}|{}^4T_1 h' M'_s\rangle \langle {}^4T_1 h' M'_s|M_q|{}^4\Gamma h M'_s\rangle}{(E({}^4T_1) - E({}^6A_1))} + \frac{\langle {}^6A_1 M_s|M_q|{}^6T_2 h'' M_s\rangle \langle {}^6T_2 h' M_s|H_{so}|{}^4\Gamma h M'_s\rangle}{(E({}^6T_2) - E({}^4\Gamma))} \tag{4}$$

electric dipole operator (x, y, and z; or in the complex representation 0, +1, and −1), M_s and M_s' are the spin sublevels, while h, h', and h'' are the orbital components of the $^4\Gamma$, $^4T_1$, and $^6T_2$ states, respectively. In eq 4, the $O \supset D_3$ basis functions[23] are used which are valid in the point group D_3. Using eqs 3 and 4, and the formalism of Piepho and Schatz,[23] the $^6A_1 \rightarrow {}^4T_1(0)$ ($^4A_2$ in D_3) transition will give rise to a positive C term, while the $^6A_1 \rightarrow {}^4T_1(\pm1)$ (^4E in D_3) transition leads to a positive pseudo A term. Only the selection rules for the $^6A_1 \rightarrow {}^4T_1$ transition are considered as this is the lowest excited state which we observe experimentally in Figure 6.

(II) Band Assignments and Energy Splittings. (a) Ligand Field Transitions. (i) Assignments. In the low-energy region of the MCD spectrum of the three complexes (Figure 6) a positive C term is observed (band 0_b). On the basis of the above selection rules this state is assigned as the $^6A_1 \rightarrow {}^4T_1(0)$ ($^4A_2$ in D_3) transition. In $[Fe(cat)_3]^{3-}$ and $[Fe(TRENCAM)]^{3-}$, a positive pseudo A term is observed (0_a) which is assigned as the $^6A_1 \rightarrow {}^4T_1(\pm1)$ (^4E in D_3) transition. The energy of the $^6A_1 \rightarrow {}^4T_1(0)$ transition corresponds to the 0_b peak maximum, whereas the energy of the $^6A_1 \rightarrow {}^4T_1(\pm1)$ transition corresponds to the 0_a crossing point. These energies and assignments are given in Table I.

(ii) Ligand Field Analysis. The value of $10Dq$ for these three complexes can be estimated from a comparison to the very similar D_3 $[Fe(oxalate)_3]^{3-}$ complex where $10Dq \approx 13\,000$ cm^{-1}, as determined from a fit of the observed $^6A_1 \rightarrow {}^4T_1$, $^4T_2$, and ^4E transitions.[25] In the $[Fe(ox)_3]^{3-}$ complex the $^6A_1 \rightarrow {}^4T_1$ transition occurs at roughly the same energy as in the tris(catecholate) complexes, indicating a similar value of $10Dq$. This assumes that the electron repulsion parameters do not change between the oxalate and catecholate complexes. The value of $10Dq$ can only be estimated as only one ligand field transition can be observed. The splitting of the $^4T_1$ can be related to the axial D_3 splitting of the octahedral t_{2g} orbitals (Figure 7) through eq 5

$$\Delta {}^4T_1 = E({}^4T_1(0)) - E({}^4T_1(\pm1)) = \frac{\delta}{2} \tag{5}$$

where δ is the splitting between the e^a and a_1 3d orbitals. The values obtained for δ from the data in Table I are given in Table III.

(25) Holt, S.; Dingle, R. *Acta Chem. Scand.* **1968**, *22*, 1091.

Table III. Comparison of Bonding Parameters (in cm^{-1})

parameter	$[Fe(cat)_3]^{3-}$	$[Fe(TRENCAM)]^{3-}$	$[Fe(eta)_3]^{3-}$
γ	3604	3495	4296
μ	7347	7193	10739
δ	2200	3200	

(b) Charge-Transfer Transitions. With the Fe 3d orbitals as an energy reference an assignment of the observed charge-transfer features can be made. From calculations on both the catechol dianion[18] and $[Fe(cat)_3]^{3-}$[15] the highest ligand valence orbitals are predicted to be $e_{\pi 1}$ and a_2 in D_3 symmetry (Figure 7). The $e_{\pi 2}$, a_1 orbitals (Figure 7) are predicted to be almost 16 000 cm^{-1} below the $e_{\pi 1}$, a_2 set.

The a_2 orbital (Figure 7) is virtually nonbonding with respect to the metal, and therefore the lowest energy charge-transfer transition in the $[Fe(cat)_3]^{3-}$ complex is predicted to be the z polarized $a_2 \rightarrow a_1$ transition. As can be seen from the polarized absorption spectrum (Figure 2), the lowest energy charge-transfer feature is the x,y polarized band which is centered at 20 500 cm^{-1}. There is no observed z polarized absorption feature in this region. This indicates that the $a_2 \rightarrow a_1$ transition is particularly weak due to the poor overlap of the ligand valence orbitals with the Fe 3d a_1 orbital. The MCD spectrum in this region (Figure 3) appears to have a negative feature associated with the x,y polarized peak in the absorption spectrum (Figure 2), with an additional positive feature to higher and lower energy. The assignment in this region can be understood by comparison between the MCD spectra of $[Fe(cat)_3]^{3-}$ (Figure 3) and $[Fe(eta)_3]^{3-}$ (Figure 5). Figure 5 reveals that the MCD in this region is actually comprised of two oppositely signed pseudo A terms. The lowest energy charge-transfer band (I) in the $[Fe(cat)_3]^{3-}$ complex exhibits a negative pseudo A term and thus must be (see Table II) the $a_2 \rightarrow e^a$ transition (Figure 7). Band II exhibits a positive pseudo A term and can be either the $e_{\pi 1} \rightarrow e^a$ or the $e_{\pi 1} \rightarrow a_1$ transition. Because the two pseudo A terms are of comparable magnitude for bands I and II these two transitions must involve the same metal e, and therefore band II must be the $e_{\pi 1} \rightarrow e^a$ transition (Figure 7). The large pseudo A term observed for bands I and II is consistent with the large magnitude of λ, expected for the metal e^a orbital. By comparison with the $[Fe(cat)_3]^{3-}$ complex, bands I and II are also assigned as the $a_2 \rightarrow e^a$ and $e_{\pi 1} \rightarrow e^a$ transitions, respectively, in the $[Fe(TRENCAM)]^{3-}$ and $[Fe(eta)_3]^{3-}$ complexes (Figures 4 and 5).

A positive MCD C term feature (band III, Figures 3–5) is observed for all three complexes. A consideration of the available transitions leaves only the $e_{\pi 1} \rightarrow e^a$, $e_{\pi 1} \rightarrow e^b$, and $a_2 \rightarrow e^b$ as possibilities (Figure 7). The $e_{\pi 2} \rightarrow e^{a,b}$, $e_{\pi 2} \rightarrow a_1$, and $a_1 \rightarrow e^{a,b}$ transitions can be ruled out based on the band VI MCD feature (Figures 3–5) which can be assigned as the $a_1(\pi_2) \rightarrow e^a$ transition (vide infra), experimentally placing the π_2 ligand valence orbitals energetically too deep to allow band III to be assigned as a $\pi_2 \rightarrow$ Fe transition (Figure 7). If band III is due to the $e_{\pi 1} \rightarrow e^a$ transition, its energy separation from band II should be small and remain relatively constant over all three complexes. Comparing the MCD spectra in Figures 3–5 reveals that the band II to band III separation increases between the $[Fe(cat)_3]^{3-}$ and $[Fe(eta)_3]^{3-}$ complexes, thus eliminating the $e_{\pi 1} \rightarrow e^a$ assignment. The $e_{\pi 1} \rightarrow e^b$ assignment for band III can be ruled out as the z and x,y polarized absorption features (bands IV and V) observed in the absorption spectrum (Figure 2) of $[Fe(cat)_3]^{3-}$ must be assigned as the $e_{\pi 1} \rightarrow e^b$ transition (vide infra). Thus band III must be the $a_2 \rightarrow e^b$ transition. The lack of a pseudo A term for this transition can be understood based on the lack of an in-state spin-orbit splitting of this state, due to the absence of angular momentum in the e^b metal orbitals. While the lack of in-state orbital angular momentum will eliminate the observation of a pseudo A term, out-of-state spin-orbit coupling will still be present leading to the observed C term in the MCD. From Figure 7 the $e_{\pi 1} \rightarrow e^b$ transition is clearly the highest energy charge-transfer transition from the π_1 set of ligand valence orbitals and must occur at higher energy than the $a_2 \rightarrow e^b$ transition. Thus bands IV and V which occur at higher energy than band III can only be assigned to the $e_{\pi 1} \rightarrow e^b$ transition. The $\pi_2 \rightarrow$ Fe transitions will occur at too high an energy to allow an assignment as bands IV and V.

All three complexes exhibit a positive pseudo A term (band VI) at roughly 37 000 cm^{-1}. On the basis of the selection rules given in Table II and the available ligand valence set (Figure 7), band VI can be assigned as the $a_1 \rightarrow e^a$ transition. The energies and assignments of all of the observed transitions are presented in Table I. Table III gives the calculated values of parameters γ and μ as defined in Figure 7. γ was determined from the energy separation between bands I and II for each complex, while μ was determined from the energy separation between bands I and III for each complex.

Discussion

The combination of low-temperature single-crystal-polarized absorption and MCD spectroscopies has allowed a definitive assignment of the electronic structure of the three iron(III) tris(catecholate) complexes studied here and, by extension, similar siderophores. Assignment of the ligand field (LF) and charge-transfer (CT) spectra (Table I) has provided an experimental energy order for the molecular orbitals of the complexes (Figure 7).

A key finding is that the broad band at 20 500 cm^{-1} in the absorption spectrum of the $[Fe(cat)_3]^{3-}$ complex, which is characteristic of the catecholate siderophores, is actually composed of two overlapping x,y polarized transitions I and II (Figures 2 and 3). Crucial to the assignment of this region of the spectrum was the observation that these two transitions are resolved in the absorption and MCD spectra of the $[Fe(eta)_3]^{3-}$ complex (Figure 5). Further support for two transitions is provided by a fit of the absorption spectrum of $[Fe(cat)_3]^{3-}$ to two Gaussian bands (not shown) at 18 414 and 22 018 cm^{-1} corresponding in energy to the two overlapping pseudo A terms in the MCD spectrum.

The energy difference between transitions I and II (designated γ in Figure 7) directly gives the amount that the $e_{\pi 1}$ orbital is stabilized relative to the ligand a_2 orbital upon forming the complex. The a_2 orbital has no metal orbital of the same symmetry close enough in energy to stabilize it significantly and is therefore virtually nonbonding. The parameter γ would then indicate the amount of π bonding in the complexes since the $e_{\pi 1}$ orbital is of the correct symmetry to be stabilized by the e^a (π^*) orbital on the metal. In all three of the complexes, γ is large (3500–4300 cm^{-1}; Table III) which indicates that there is substantial π bonding in the tris(catecholates); i.e., the oxygen lone pairs which are out-of-plane relative to the catechol ring overlap significantly with the corresponding metal e^a orbitals derived from the t_{2g} set in O_h. Further evidence that π bonding is very significant is the large extinction coefficients seen for the ligand π-to-metal CT transitions ($\epsilon \sim 4000$ M^{-1} cm^{-1}). For $[Fe(eta)_3]^{3-}$, there is a 600-cm^{-1} increase in γ, which indicates a greater degree of π bonding in this complex.

The measured energy difference between transitions I and III gives the parameter μ, which is the separation between the two metal orbitals e^a and e^b (Figure 7). Since the e^b orbital is derived from the e_g (σ^*) set in O_h and is therefore destabilized upon σ bonding, μ is a direct measure of the amount of σ bonding in the complexes. From Table III there is an $\sim$3500-cm^{-1} increase in μ for $[Fe(eta)_3]^{3-}$ indicating that eta^{2-} is a better σ bonding ligand to Fe^{III} than either cat^{2-} or $TRENCAM^{6-}$. Since the pK_as for the hydroxyl protons in H_2eta[7] are 6 and 11, whereas they are 9 and 13 for H_2cat,[5] it might have been predicted a priori that eta^{2-} would be a poorer σ bonding ligand; i.e., the Lewis basicity of the catecholate oxygens in eta^{2-} would have been anticipated to be lower relative to cat^{2-} based on the pK_as. This argument however is not sound considering the following: Since the pK_as of each ligand indicate the relative stability of the *anion* in H_2O, there is not a clear parallel between the pK_a values and σ bonding. In eta^{2-}, the anion can be stabilized significantly due to hydrogen bonding from the amide protons to the catecholate oxygens,[7] which lowers the pK_as. In addition, the σ bonding to a proton cannot be directly compared to the σ bonding to metal d orbitals since

overlap considerations are significantly different.

To the extent that final state relaxation is similar for the charge-transfer excited states, these features determined spectroscopically will reflect bonding in the ground state. From a comparison of the bonding parameters γ and μ (Table III), it is clear that the complexes $[Fe(cat)_3]^{3-}$ and $[Fe(TRENCAM)]^{3-}$ have similar electronic structures, whereas the Fe–O bonding in $[Fe(eta)_3]^{3-}$ appears to have a larger degree of both σ and π interactions. Considering that the thermodynamic stability data are available for these complexes, one can address whether these differences in bonding contribute significantly to the measured stability constants. One might predict that $[Fe(eta)_3]^{3-}$ would have a larger stability constant than $[Fe(cat)_3]^{3-}$. In fact, the reverse is true; the overall stability constant, log K_f, for $[Fe(eta)_3]^{3-}$ is 42.2[7] and for $[Fe(cat)_3]^{3-}$ is 43.7 although the η complex is relatively more stable at pH 7.[5] However, considering that the hydration enthalpies of these ligand and complex species are very large, it becomes clear that small differences in the stability of similar ligand–metal complexes cannot be directly related to quantitative differences in bonding. Nevertheless, the fact that these stability constants are so large relative to, for example, $[Fe(ox)_3]^{3-}$ (log K_f = 18)[26] *can* be attributed to the large degree of π bonding determined spectroscopically (vide supra).

From the energies of the LF transitions 0_a and 0_b observed in the MCD, a value of $10Dq \approx 13000$ cm^{-1} was determined for the iron(III) tris(catecholates), in addition to the low symmetry splitting parameter (δ) of the t_{2g} set of d orbitals (Figure 7). This value of $10Dq$ is very close to that which is empirically calculated[27] for iron(III) with six (OH^-) ligands: 13 160 cm^{-1}. From Figure 7 it can be seen that a calculation of $10Dq$ can also be made from the CT transition energies. If the center of gravity between the a_1 and e^a metal orbitals is taken to be an approximation of the t_{2g} energy level, then $\mu + (1/3)\delta$ should be equal to $10Dq$. Calculating $10Dq$ in this way results in the values 8080 cm^{-1} for $[Fe(cat)_3]^{3-}$ and 8260 cm^{-1} for $[Fe(TRENCAM)]^{3-}$ (δ was not determined for $[Fe(eta)_3]^{3-}$; see Results section). The fact that these values differ substantially from 13 000 cm^{-1} can be understood considering that, upon ligand-to-metal charge transfer, the excited state is best described as a $[Fe^{II}(semiquinone)(cat)_2]^{3-}$ species. The value of $10Dq$ for a Fe^{II} complex should be ~70% of the value for a Fe^{III} complex with identical ligands.[27] The value that we calculate for $10Dq$ based on the CT transitions is ~63% of the value determined from the LF transitions. This then provides spectroscopic proof that the CT excited state is best considered as an iron(II) species produced in an internal redox reaction.

As mentioned in the Introduction, a theoretical study of the $[Fe(cat)_3]^{3-}$ species previously predicted that the ground state would best be described as low spin (S = 1/2).[15] The present investigation of the CT and LF spectra of $[Fe(cat)_3]^{3-}$ supports the magnetic, EPR, and Mössbauer data, which show that the complex is in fact high-spin iron(III) (S = 5/2).

These studies have shown that the CT bands in the iron(III) tris(catecholates) arise from ligand π-to-metal d transitions. The results demonstrate that a significant contribution to the Fe–O interaction is made by π bonding and that this can account for the high stabilities of these complexes relative to similar Fe^{III} complexes (e.g., $[Fe(ox)_3]^{3-}$). We have determined spectroscopically that the CT excited state is best described as an iron(II) species. Furthermore, since the spectroscopic properties of enterobactin are essentially identical with the TRENCAM complex studied here, the present analysis is directly applicable to the biologically important catechol siderophores.

Acknowledgment. We would like to thank Professor T. D. Westmoreland for helpful discussions through the initial phases of this work. Also, the National Institutes of Health (Grant AI 11744 to K.N.R. and GM 40392 to E.I.S.) is thanked for support of this research.

Registry No. $K_3[Fe(cat)_3]$, 32963-76-1; $[Fe(ent)]^{3-}$, 61481-53-6; $[Fe(TRENCAM)]^{3-}$, 131933-38-5; $[Fe(eta)_3]^{3-}$, 132376-23-9; $K_3[Fe(eta)_3]$, 132376-24-0; H_2eta, 117918-05-5; $(Et_3NH)_3[Fe(TRENCAM)]$, 132376-26-2; $H_6TRENCAM \cdot HBr$, 107959-86-4; $Fe(acac)_3$, 75025-36-4; Fe_2O_3, 1309-37-1; Fe, 7439-89-6.

(26) Deneux, M.; Meilleur, R.; Benoit, R. L. *Can. J. Chem.* **1968**, *46*, 1383.

(27) Figgis, B. N. *Introduction to Ligand Fields*; Krieger: FL, 1986.